Appl Nanosci (2012) 2:261–273
DOI 10.1007/s13204-012-0103-y

ORIGINAL ARTICLE

Magnetoelectric properties of $PbZr_{0.53}Ti_{0.47}O_3$–$Ni_{0.65}Zn_{0.35}Fe_2O_4$ multiferroic nanocomposites

D. K. Pradhan · R. N. P. Chowdhury · T. K. Nath

Received: 21 November 2011 / Accepted: 22 March 2012 / Published online: 11 April 2012

Abstract A different kind of multiferroics with ferroelectric–ferrimagnetic (FE–FM) composites: $(1 - x)$ $PbZr_{0.53}Ti_{0.47}O_3$–x $Ni_{0.65}Zn_{0.35}Fe_2O_4$ with $x = 0.10$, 0.20 and 0.30, were synthesized by a powder-in-sol precursor hybrid processing route. Structural analysis with X-ray diffraction (XRD) data revealed the presence of both $PbZr_{0.53}Ti_{0.47}O_3$ (PZT) and $Ni_{0.65}Zn_{0.35}Fe_2O_4$ (NZFO) pure phases in the PZT–NZFO composites. Scanning electron micrographs (SEM) clearly disclose distribution of both PZT and NZFO phases throughout the sample. Dielectric and electrical properties of the system have been investigated in a wide range of frequency at different temperatures. Dielectric constant (ε_r) as a function of temperature reveals the paraelectric–FE transition temperature at ~408 °C having maximum value of ε_r at the peak [$\varepsilon_r^{max} = 1{,}200$] with another low temperature anomaly at ~297 °C, very close to the magnetic Curie temperature of the NZFO ferrite ($T_c = 300$ °C) for the $x = 0.1$ FE–FM composite. The impedance spectroscopy data of these composites show clearly, contribution of both grain and grain boundary effect in the electrical properties of the composites. Negative temperature coefficient of resistance (NTCR) behavior of the materials indicates their semiconducting nature. The ac conductivity spectrum is found to obey Johnscher's power law very well. The temperature-dependent magnetization hysteresis (M–H) loops of the PZT/NZFO composite show excellent non-saturating ferrimagnetic behavior with increase in both coercive field (H_c) and remanent magnetization (M_r) when the NZFO content in the composite is increased. Polarization (P) versus electric field (E) studies at 300 K give conclusive evidence of the presence of spontaneous polarization in all the three composites ($x = 0.1$, 0.2 and 0.3). However, area of P–E loop, coercive field (E_c) and remanent polarization (P_r) are found to decrease noticeably with the increase of the NZFO content (x) in these composites.

Keywords Ferroelectrics · Spinel ferrites · Multiferroics · Dielectrics · Impedance spectroscopy

D. K. Pradhan · R. N. P. Chowdhury · T. K. Nath (✉)
Department of Physics and Meteorology, Indian Institute of Technology, Kharagpur, West Bengal 721302, India
e-mail: tnath@phy.iitkgp.ernet.in

Introduction

Recent thrust on developing multifunctional for high performance solid state device applications is a driving force to work on multiferroics materials (Eerenstein et al. 2006; Spaldin and Fiebig 2005; Prellier et al. 2005). Multiferroic materials that combine spontaneous magnetization (M_S) with ferroelectric polarization (P_S) are of tremendous technological and fundamental interest. The strong coupling between M_S and P_S would allow ferroelectric (FE) data storage combined with a magnetic read and the ability to tune the magnetic properties with an electric field and vice versa. Multiferroics are those materials, which possess more than two primary ferroic order parameters (i.e., charge, spin and strain) in a single-phase material so that it can enable to tune magnetization by the application of electric field and vice versa (Spaldin and Fiebig 2005). This effect is called magnetoelectric effect. Due to the coexistence of more than one ferroic order parameters (mainly spontaneous polarization (P_s), magnetization (M_s), strain etc.), these materials have received a considerable attention for various multifunctional devices such as multiple-state memory elements, electric field controlled ferromagnetic resonance devices, transducers, spintronics and

terahertz radiation etc. (Eerenstein et al. 2006; Prellier et al. 2005). Due to the mutual exclusiveness of ferroelectric and ferromagnetic ordering, there are only a few single-phase mutiferroic materials such as $BiFeO_3$, $BiMnO_3$, etc. (Prellier et al. 2005) available today. Unfortunately, some inherent problems and challenges, namely (1) difficult to fabricate the single-phase materials, (2) high leakage current and dielectric loss, (3) low electromagnetic coupling coefficient, (4) structural distortion and (5) low temperature phase transitions etc. (Lee et al. 2006; Choudhary et al. 2006) are associated to obtain suitable materials for applications. Though various research activities have been initiated by different research groups around the globe to overcome the above problems, not much success has been achieved on enhancing the electromagnetic coupling coefficient. The magnetoelectric coupling coefficient occurs either directly between the two order parameters or indirectly via strain (Ramesh and Nicola 2007; Ryu et al. 2007). Moreover, it has been found that FE ferromagnet in single-phase materials with large and robust MS and PS is rare; they tend to exhibit rather weak ferromagnetism or are not strong enough insulators to sustain FE polarization at room temperature. In fact, the coexistence of ferroelectricity and ferromagnetism is difficult to achieve in single-phase materials. Alternatively, multiferroic composites are likely to possess a large magnetoelectric coupling factor with high value of M_S and P_S, which is desirable for device applications as compared to the single-phase counterpart. The strong magnetoelectric coupling factor is due to effective strain-mediated ME coupling giving rise to the giant product property of the piezoelectric and magnetostrictive effect of both the components (Martin et al. 2008; Singh et al. 2006; Miao et al. 2005; Mathews et al. 1997). To obtain maximum electromagnetic coupling coefficient, various composite systems have been fabricated and characterized in different forms such as, (1) multilayer nano-structured thin film of ferroelectric and magnetic oxides, (2) bulk composite in 0–3 connectivity (where second phase particles embedded in a primary matrix phase), (3) three phase ME composites of ferroelectric and ferromagnetic oxides dispersed in polymer matrix and (4) 1–3 self-assembled ME composite thin films consisting of FE or FM nanopillars embedded in a FM or FE matrix by several research groups (Martin et al. 2008; Singh et al. 2006; Miao et al. 2005; Mathews et al. 1997; Catlan and Scott 2009; Martínez et al. 2010; Zheng et al. 2004; Yan et al. 2010). In view of the above, several attempts have been made by researchers to develop different types of new composites, some of them are mentioned below.

Zhang et al. (2008) prepared $Ni_{0.5}Zn_{0.5}Fe_2O_4$–$PbZr_{0.53}Ti_{0.47}O_3$ (NZFO/PZT) ceramic by dispersion of nano-sized NZFO ferromagnetic powder into PZT ferroelectric ceramics. The composite showed simultaneous effect of ferromagnetic and ferroelectrics at room temperature with excellent dielectric and magnetic properties. Magnetoelectric composites of $x\ Ni_{0.9}Zn_{0.1}Fe_2O_4 + (1 - x)\ PbZr_{0.52}Ti_{0.48}O_3$ (NZFO/PZT) with a wide range of x have been prepared by Chougule et al. (2008). They observed the maximum value of magnetoelectric voltage coefficient for 15 % NZFO in 85 % PZT. Impedance spectroscopy studies of $PbZr_{0.53}Ti_{0.47}O_3$–$CoFe_2O_4$ (PZT/CFO) multilayer thin film have been studied by Ortega et al. (2008). Vaz et al. (2010) studied the magnetoelectric response of $PbZr_{0.2}Ti_{0.8}O_3$–$La_{0.8}Sr_{0.2}MnO_3$ (PZT/LSMO) multiferroic heterostructure as a function of temperature and magnetic field. They observed the maximum magnetoelectric coupling coefficient near the magnetic critical point of LSMO. One dimensional multiferroic $NiFe_2O_4$–$PbZr_{0.52}Ti_{0.48}O_3$ core shell nano-wire array has been synthesized by Liu et al. (2007) using modified sol–gel process and electro-deposition techniques. Magnetoelectric coupling effects in a submicron thick of $PbZr_{0.52}Ti_{0.48}O_3$–$La_{0.7}Sr_{0.3}MnO_3$ (PZT/LSMO) composite film have been investigated by Ma et al. (2007). Wu et al. (Yujie 2008) synthesized and characterized $BiFeO_3$–$PbZr_{0.52}Ti_{0.48}O_3$ (BFO/PZT) composite film where BFO nanoparticles were distributed in PZT matrix. Direct coupling between ferroelectric and ferromagnetic ordering in BFO, and ferroelectric and ferromagnetic coupling between BFO and PZT are found to be responsible for the magnetoelectric effect in the composite film. Chen et al. (Chen et al. 2010a) fabricated a thick film composite of $CoFe_2O_4$/$PbZr_{0.53}Ti_{0.47}O_3$ (CFO/PZT) assisted by polyvinyl pyrrolidone (PVP) employing a hybrid sol–gel processing and spin coating technique. They observed low value of magnetoelectric coupling coefficient due to the porous microstructure of the materials. Zhang et al. (2009) characterized fine grained multiferroic of $BaTiO_3$/$Ni_{0.5}Zn_{0.5}Fe_2O_4$ (BTO/NZFO) composite ceramics synthesized by novel powder-in-sol precursor hybrid processing route. Harnagea et al. (2007) prepared $BaTiO_3$/$Ni_{0.5}Zn_{0.5}Fe_2O_4$ (BTO/NZFO) composite by co-precipitation process. They observed the multiferroic character at nanoscale due to the presence of magnetic and ferroelectric domain structure in the same region. Fawzi et al. (2010) studied the ferroelectric, ferromagnetic and magnetoelectric properties of $x\ NiFe_2O_4 + (1 - x)\ Pb_{0.93}La_{0.07}(Zr_{0.53}Ti_{0.47})O_3$ (NFO/PLZT) composite by double sintering ceramic method. Chen et al. (2009) studied the impedance spectroscopy and the conductivity mechanism of the $CoFe_2O_4$/$PbZr_{0.53}Ti_{0.47}O_3$ (CFO/PZT) composite thick film. Chen et al. (Chen et al. 2010b) prepared the thick film of $Ni_{0.5}Zn_{0.5}Fe_2O_4$/$PbZr_{0.53}Ti_{0.47}O_3$ and studied their magnetic and ferroelectric properties.

In this work, we have investigated the multiferroic properties of the PZT–NZFO composites (with varying NZFO content) through dielectric, electrical, magnetization and polarization measurements for possible technological applications. No single-phase ferromagnetic and

ferroelectric materials with high value of M_s and P_s were found so far. Therefore, an attempt is being made here to study the multiferroic properties in composites having both high value of FE and FM character. The Ni–Zn ferrites are magnetically soft (i.e., possess high saturation magnetization, low coercivity, high resistivity, high magnetostriction coefficient and low dielectric losses) (Mangalaraja et al. 2002). The Ni–Zn ferrite system with a stoichiometric composition $Ni_{0.65}Zn_{0.35}Fe_2O_4$ has been chosen for the present investigation as this composition exhibits the highest saturation magnetization in the entire Ni–Zn series. The solid solution of lead titanate and lead zirconate in a ratio of 47:53 ($PbZr_{0.53}Ti_{0.47}O_3$) shows very high dielectric value, high piezoelectric constant and pyroelectric properties, for which they became the most studied material in single crystal, ceramic and thin film forms (Uchino 2000). This has motivated us to study the dielectric, electrical, magnetic and ferroelectric properties of PZT–NZFO composites.

Experimental details

The $(1 - x)$ $PbZr_{0.53}Ti_{0.47}O_3$–x $Ni_{0.65}Zn_{0.35}Fe_2O_4$ [$x = 0.10$ (abbreviated as PN 1), 0.20 (abbreviated as PN 2), 0.30 (abbreviated as PN 3)] composites were synthesized by a powder-in-sol precursor hybrid processing route. The polycrystalline samples of $PbZr_{0.53}Ti_{0.47}O_3$ (PZT) ceramic were first synthesized by a high-temperature solid-state reaction route using high-purity (99.9 %) oxide precursors; PbO, ZrO_2 and TiO_2 in required stoichiometry. The above ingredients were first mixed thoroughly in a mortar and pestle in air atmosphere for 3 h and then in methonol in 1 h. The process of grinding and calcination was repeated until the formation of a single-phase compound was confirmed by X-ray diffraction technique. Finally, the compound was calcined at an optimized temperature (1,150 °C) for 6 h. Further, for the synthesis of $Ni_{0.65}Zn_{0.35}Fe_2O_4$, nickel nitrate ($Ni(NO_3)_3.6H_2O$), zinc nitrate ($Zn(NO_3)_3.6H_2O$), iron(III) nitrate ($Fe(NO_3)_3.9H_2O$), citric acid ($C_6H_8O_7.H_2O$) and de-ionized water were used. The precursors were weighed according to the required stoichiometry. Appropriate amount of metal nitrates and citric acid was dissolved in minimum amount of de-ionized water to make a clear solution. A molar ratio 1:1 of nitrates to citric acid was used. A small amount of ammonia is added to it to adjust the pH value at about 7. The solution is continuously stirred using magnetic stirrer during this procedure. Then the mixed solution is heated and stirred continuously to form a gel like material. In an appropriate temperature ignition starts and dried gel burns in a self-propagating combustion until all the gel burns out completely to form a loose powder. This mixture was evaporated to obtain dry and homogeneous uniformly colored brown transparent glassy material. Then the powder was calcined at an optimized temperature of 500 °C for 6 h. After preparation of both the powders, the calcined fine powders of $PbZr_{0.53}Ti_{0.47}$ O_3 and $Ni_{0.65}Zn_{0.35}Fe_2O_4$ were mixed in different volume fractions (90:10, 80:20, 70:30 wt%) thoroughly by grinding and calcined them at an optimized temperature (550 °C) for 6 h. Then the PZT–NZFO powder was mixed with polyvinyl alcohol (PVA as binder) and pressed into cylindrical pellets of 10 mm diameter, under an isostatic pressure of 5×10^6 Nm^{-2} using a hydraulic press. Then the pellets were sintered at an optimized temperature of 800 °C for 6 h in air in a platinum crucible. PVA was completely burnt out during this high-temperature sintering process.

To check the phase formation and quality of the compound, we have carried out a high resolution X-ray diffraction (HRXRD) analysis at room temperature with a powder diffractometer (PW-1710) using CoK_α radiation ($\lambda = 1.78897$ Å) in a wide range of Bragg's angles θ ($20^o \leq 2\theta \leq 80^o$) at a scanning rate of 3^o/minute. A sintered pellet was polished with fine emery paper, coated finally with conductive silver paint and dried at 150 °C for 4 h prior to carrying out the electrical measurements. The dielectric and electrical (impedance, electrical modulus etc.) properties of the sample were measured using a computer-controlled LCR meter (N4L: PSM1735) in the frequency range of 10^2–10^6 Hz at different temperatures (30–500 °C). Magnetic measurements of the samples were carried out using a laboratory-fabricated vibrating sample magnetometer (VSM) set up in a temperature range of 80–300 K with a maximum magnetic field of 500 Oe. Signal has been detected employing a DSP Lock-In-Amplifier (SR830). Temperature measurement and controlling have been done employing a high-precision temperature controller (Lakeshore, 331S) with better than ±50 mK temperature stability.

Results and discussion

To check the phase purity of calcined powder of pure PZT, pure NZFO and PZT–NZFO composites (i.e., PN 1, PN 2 and PN 3), X-ray diffraction patterns have been recorded at room temperature as shown in Fig. 1. The presence of sharp and well defined peaks for PZT and NZFO is the characteristic peaks of perovskite and spinel phases, respectively (Zhang et al. 2008). The peaks were indexed with the reported crystal structure using the JCPDS X-ray diffraction files and least-squares refinement software. No impurity phase has been detected in PZT and NZFO samples. In the case of composites, X-ray diffraction patterns reveal the presence of both PZT and NZFO binary phase. It has been noticed that the intensity of the peak corresponding to the ferrite spinel phase keeps on

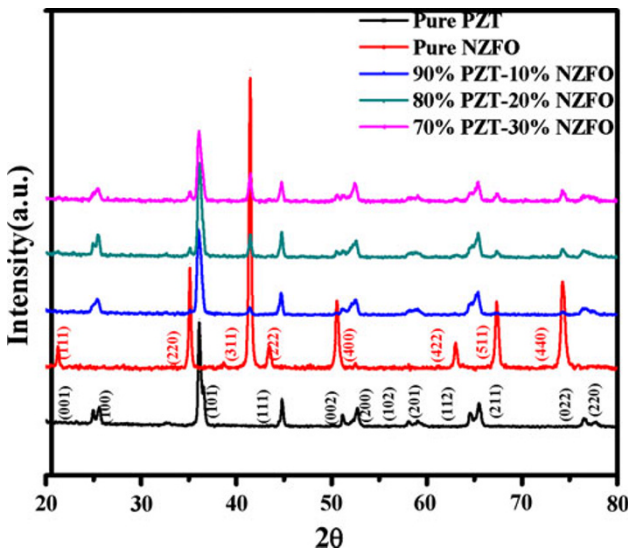

Fig. 1 Room temperature XRD pattern of $PbZr_{0.53}Ti_{0.47}O_3$, $Ni_{0.65}Zn_{0.35}Fe_2O_4$ and $(1 - x)$ $PbZr_{0.53}Ti_{0.47}O_3$–x $Ni_{0.65}Zn_{0.35}Fe_2O_4$ for different value of x. $x = 0.10$, 0.20 and 0.30

increasing with increase in ferrite concentration. It is also confirmed that no intermediate phase has been detected in the XRD pattern. The position of the most intense peak has negligible shift with varying composition (x) and the relative intensities of the two peaks systematically change with x. This observation indicates an almost complete immiscibility of NZFO and PZT within the mixture.

To investigate the microstructure and morphology of PZT–NZFO (PN 1, PN 2, PN 3) composites SEM micrographs have been recorded at room temperature as shown in Fig. 2. The microstructures of the sintered pellets show that grain growth process is more or less completed during the sintering process. The microstructure is overall dense, but few scattered pores are observed which indicates that there is certain degree of porosity in the sample. SEM micrographs show the polycrystalline nature of microstructures with different grain size which are inhomogenously distributed throughout the sample surface. Mainly two different sized grains are observed; (1) one having average grain size of 2–4 μm and (2) second one corresponds to grains having grain size less than 1 μm to tens of nm dimension. The first category of grains represents the morphology of PZT and second category represents that of NZFO. The distribution of the two phases in the composites is non uniform. It is very much clear that grains of PZT (2–5 μm grains) dominate in the micrograph, which shows the higher amount of PZT content in the composites.

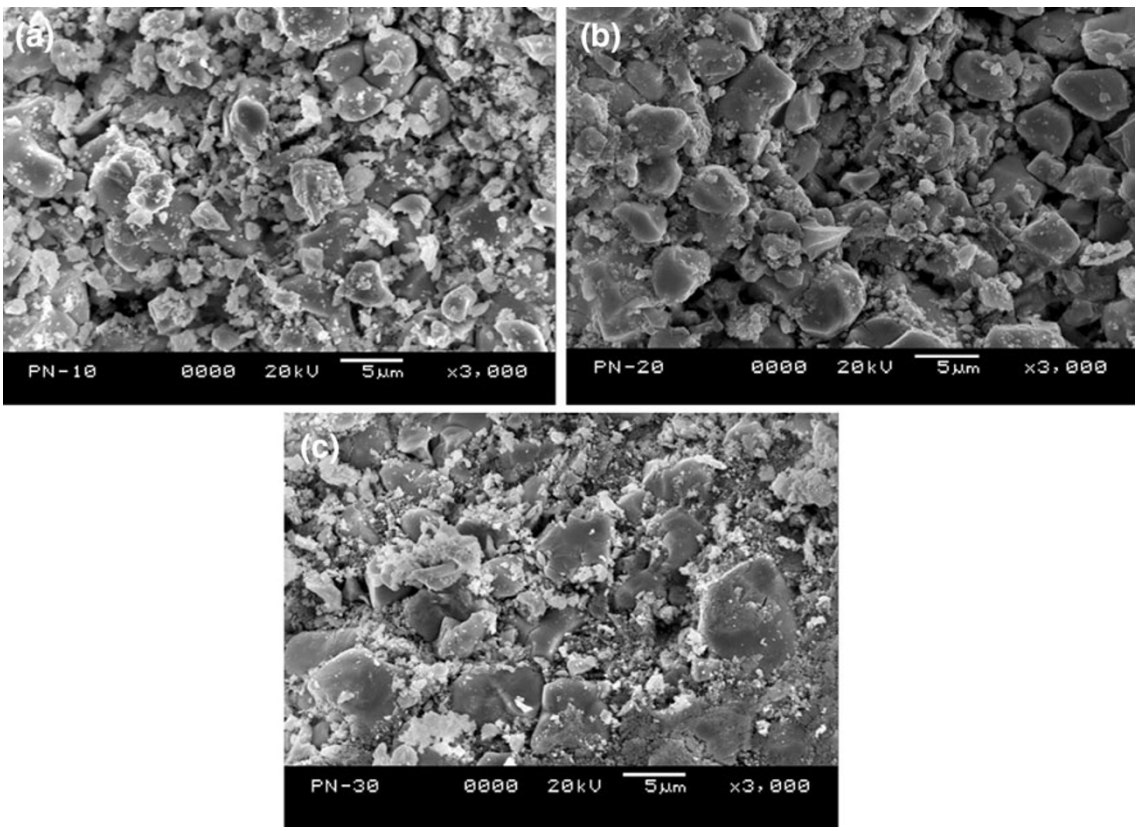

Fig. 2 Room temperature SEM of $(1 - x)$ $PbZr_{0.53}Ti_{0.47}O_3$–x $Ni_{0.65}Zn_{0.35}Fe_2O_4$ for different value of x, **a** $x = 0.10$, **b** 0.20 and **c** 0.30 at a magnification (×3,000)

The average grain size increases with increase in NZFO content.

Figure 3 shows the variation of relative dielectric constant (ε_r) as a function of temperature at different frequencies for PN 1, PN 2, PN 3 composites, respectively. It has been observed that the relative dielectric constant decreases with increase in frequency irrespective of composition, which is a typical characteristic of most of the polar dielectrics (Kao 1992). It has also been observed that the value of ε_r of these composites first increases with increase in temperature, reaches to its highest (peak) value, and then decreases. The peaks of these plots indicate the FE–paraelectric transition temperatures (Curie temperatures). The trend of variation of ε_r with temperature of these compounds is different for different compositions. For PZT, the reported Curie temperature is around 387 °C (Uchino 2000). In the case of PN 1 sample (10 % NZFO in 90 % PZT matrix), the Curie temperature was found to be 408 °C, with another low temperature anomaly observed around 297 °C. This observed low temperature anomaly is very close to the magnetic (ferrimagnetic–paramagnetic transition) Curie temperature (~300 °C) of NZFO. Similar change in permeability close to this transition temperature has also been reported earlier in NZFO system. This new low temperature anomaly in dielectric measurement of this ferroelectric composite is confirmed to be very close to its magnetic transition (Curie) temperature, which strongly suggests reasonably high magnetoelectric coupling in these PZT/NZFO composite samples. In the case of PN 2 sample, high temperature peak is found to be very small and the low temperature anomaly (293 °C) becomes more prominent. In the case of PN 3, no drastic variation in Curie temperature is observed as compared to PN 2. The observed transition temperature and maximum value of dielectric constant at a frequency of 10 kHz for all the three samples are listed in Table 1. The decrease in Curie temperature with increase in NZFO content is in agreement with the results obtained by Zhang et al. (2008). It is also observed that the value of permittivity decreases on increasing NZFO content.

Figure 4 shows the variation of tangent loss as a function of temperature at different frequencies for the PZT–NZFO (PN 1, PN 2 and PN 3) composites. For PN-1, the value of tanδ of this composite becomes almost constant up to 300 °C, and then starts increasing on further increase of temperature. For PN-2 and PN-3 composites, the tangent loss increases with increase in temperature, and showed a peak around 300 °C. At high temperatures the value of tanδ again increases with rise in temperature. This increasing trend in tanδ in the high temperature and low frequency regions may be due to space charge polarization. The appearance of anomaly/peak in tanδ versus temperature graph is nearly the same as observed in temperature-dependent dielectric constant plot.

Figure 5a, b and c illustrates the frequency response of imaginary part of impedance for PZT–NZFO (PN 1, PN 2

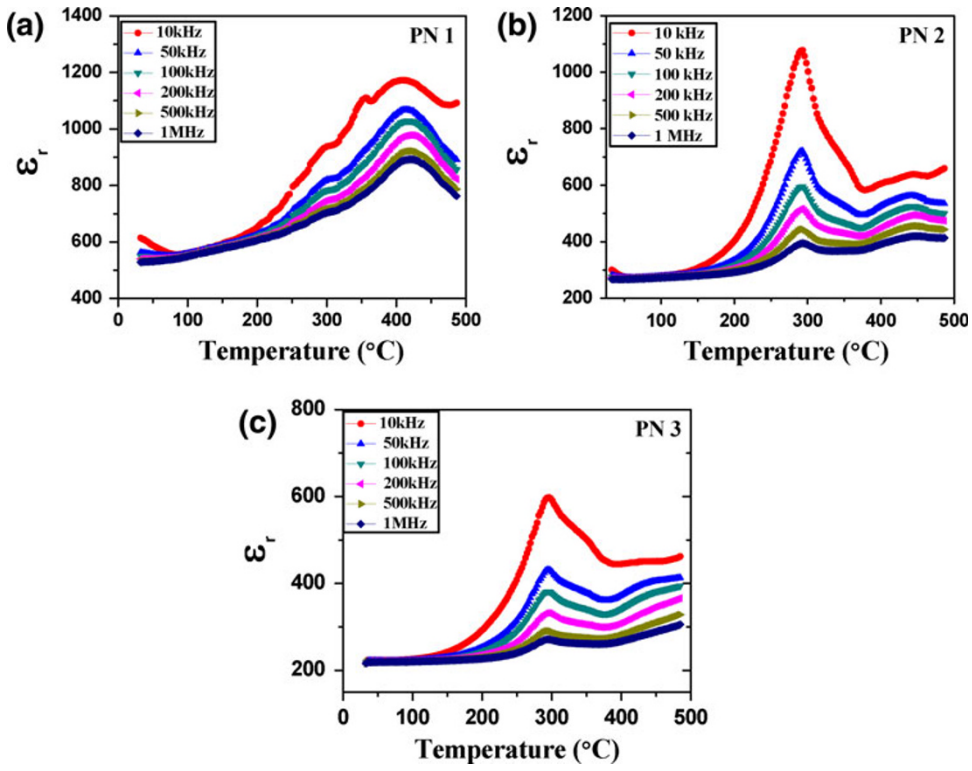

Fig. 3 Variation of relative dielectric permittivity with temperatures at different frequencies for $(1 - x)$ $PbZr_{0.53}Ti_{0.47}O_3$–x $Ni_{0.65}Zn_{0.35}Fe_2O_4$ composites for different value of x **a** $x = 0.10$, **b** 0.20 and **c** 0.30

Table 1 Transition temperature and maximum value of dielectric constant of $PbZr_{0.53}Ti_{0.47}O_3$–$Ni_{0.65}Zn_{0.35}Fe_2O_4$ composites at 10 kHz

Sample	Dielectric constant	T_c (°C)
PN 1	1,173	408
PN 2	1,078	293
PN 3	598	296

and PN 3) composites. The Z'' versus frequency patterns exhibit some important features of the composites such as (1) a monotonous decrease in Z'' with a rise in frequency (within the investigated frequency range at low temperatures), (2) appearance of a peak at a particular frequency (known as relaxation frequency), (3) decrease in the magnitude of Z'' with a clear shift in the peak frequency toward higher frequency, and (4) peak broadening with a rise in temperature. The peak location gives the relaxation time according to the relation $\omega_{max}\tau = 1$, where ω_{max} is the angular frequency at the maximum of Z''-f (frequency) patterns. Moreover, the frequency of the maxima (an apparent relaxation frequency) shifts to its higher value on increasing temperature. These behaviors may be understood due to the temperature dependence of electrical relaxation phenomena on the materials (Pradhan et al. 2009). The effect of NZFO content on PZT can be clearly observed as, (1) appearance of relaxation peak at low temperatures, (2) increase in magnitude of Z''_{max}, and (c) decrease in relaxation frequency (for a particular temperature). We have also calculated the relaxation frequency from the peak position of Z'' with frequency plots at different temperatures from Fig. 5a, b and c for all the three samples. The relaxation times (τ) are calculated using the relation as $2\pi f_r\tau = 1$, where f_r is the relaxation frequency. The ln(τ) versus 1/T plot for all the three samples shows linear behavior (Fig. 5d). The typical variation appears to be of Arrhenius nature governed by the relation $\tau = \tau_o \exp(E_a/k_BT)$, where k_B is the Boltzmann constant, τ_o is the pre-exponential factor and E_a is the activation energy. From the Arrhenius fits the activation energy for all the three samples has been estimated to be $E_a = 0.94$, 0.99 and 1.09 eV for $x = 0.1$, 0.2 and 0.3, respectively. From these temperature-dependent electrical relaxation phenomena, it appears that with the increase of NZFO content (x) in these multiferroic composite materials the activation energy (E_a) is slightly enhanced.

The complex impedance spectra (Nyquist-plots) of the composites measured at different temperatures are shown in Fig. 6. The complex impedance plot typically comprises of a single semicircular arc at low temperatures with center below the real axis suggesting the departure from ideal Debye behavior (Macdonald 1987). The semicircular arcs are gradually resolved with increase in temperature. At low temperatures, only one semicircular arc has been observed whereas at

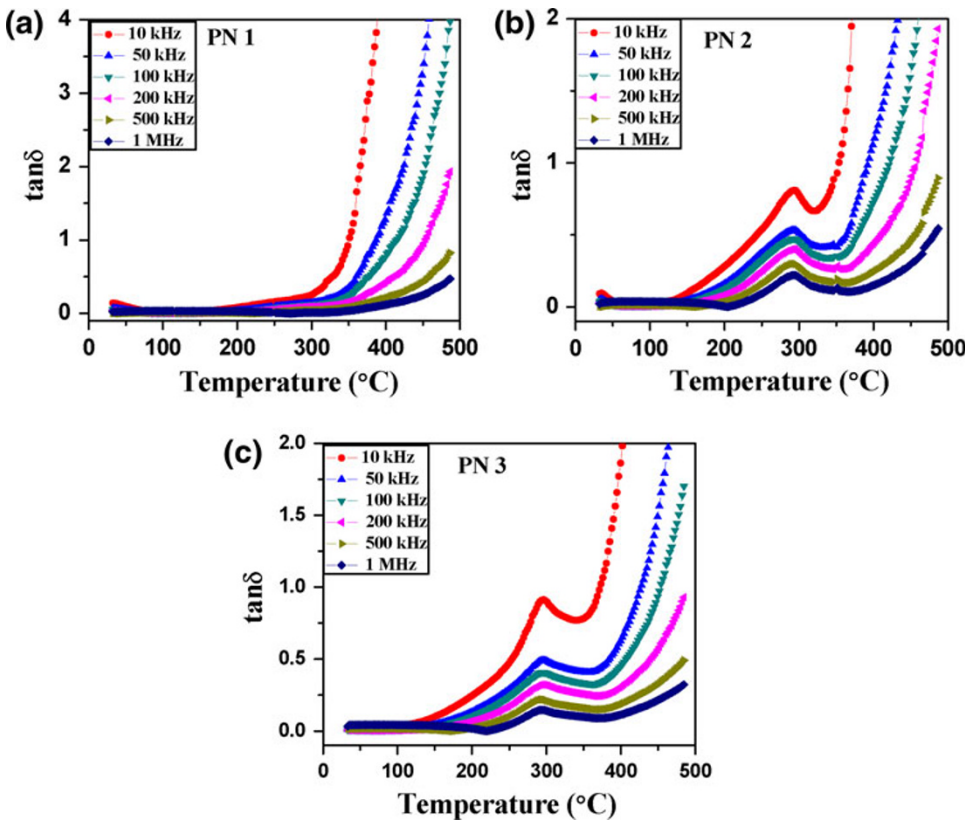

Fig. 4 Variation of tanδ with temperatures at different frequencies for $(1 - x)$ $PbZr_{0.53}Ti_{0.47}O_3$–x $Ni_{0.65}Zn_{0.35}Fe_2O_4$ composites for different value of x, **a** $x = 0.10$, **b** $x = 0.20$ and **c** $x = 0.30$

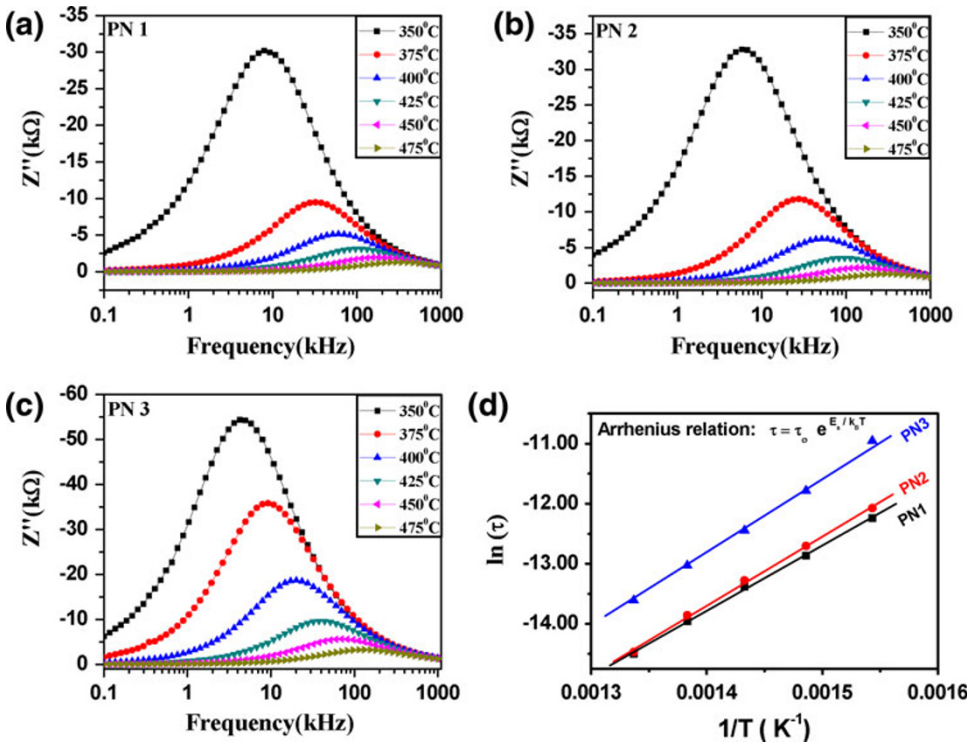

Fig. 5 Variation of imaginary part of complex impedance (Z'') with frequency at various temperatures of $(1 - x)$ $PbZr_{0.53}Ti_{0.47}O_3$–x $Ni_{0.65}Zn_{0.35}Fe_2O_4$ composites for different value of x, **a** $x = 0.10$, **b** 0.20 and **c** 0.30. **d** Variation of relaxation time (τ) as a function temperature and the best fits with Arrhenius relation $\tau = \tau o \exp(E_a/K_B T)$ for all the three samples

higher temperatures two overlapping semicircular arcs have been observed. The observed single semicircular arc at low temperatures is the contribution of the grain (bulk) properties of the material. The presence of two overlapping semicircular arcs represents the contribution of both bulk and grain boundary effect. An equivalent circuit is commonly used in impedance spectroscopy analysis to establish the structure–property relationship of the materials. In the present work, two overlapping semicircular arcs of the impedance spectra have been modeled to an equivalent circuit (as shown in Fig. 6) of a parallel combination of (1) a resistance (bulk resistance), capacitance (bulk capacitance) and a constant phase element (CPE) connected in series with (2) a parallel combination of a resistance (grain boundary resistance), capacitance (grain boundary capacitance) (Pradhan et al. 2009). Figure 6 compares the complex impedance plots (symbols) with fitted data (solid line) using commercially available software ZSimp Win Version 2 for all the three samples at various temperatures. There is a close agreement between the experimental and fitted data justifying the correctness of choosing the circuit as shown in Fig. 6. All the temperature-dependent electrical parameters (R_b (Ω), C_b (F), R_{gb} (Ω) and C_{gb} (F)) obtained from the fitting using the equivalent circuit model to the measured data at different temperatures of $(1 - x)$ $PbZr_{0.53}Ti_{0.47}O_3$–x $Ni_{0.65}Zn_{0.35}Fe_2O_4$ composites have been summarized in Table 2 for comparison.

Figure 7 shows the frequency response of imaginary part of complex impedance (Z'') and complex electrical modulus (M'') of PZT–NZFO composites (i.e., PN 1, PN 2, PN 3) at 400 °C. For a Debye type relaxation, the peak of the both impedance and modulus plots should coincide. Any departure from this shows the non-Debye type relaxation. From these plots the Z'' and M'' peaks are not coinciding, which indicates the departure from Debye relaxation in PN 1 sample. It is also observed that with increase in NZFO content, the peak separation increases which suggests gradual departure from Debye ideality (Macdonald 1987; Lanfredi et al. 2000; West et al. 1997). The departure from the ideality justified the presence of constant phase element (CPE) in the circuit. Impedance of CPE is given by, $Z_{CPE} = [A_0(j\omega)^n]^{-1}$ where, $A_0 = A/\cos(n\pi/2), j = \sqrt{-1}$. A and n are the frequency-independent parameters which usually depend on temperature. As n represents the gradient of the linear dispersion region of conductivity spectra, it is the power law exponent in Jonscher's power law. The value of n lies between 0 and 1 ($n = 1$ for an ideal capacitor and $n = 0$ for an ideal resistor) (Macdonald 1984).

The variation of imaginary part of electrical modulus (M'') with frequency at different temperatures is shown in Fig. 8. It is observed that M'' decreases with increase in frequency at lower temperatures, whereas the modulus spectra showed peaks with rise in temperature. Above 200 °C, the variation of M'' with frequency attains two maxima in the lower frequency and higher frequency regions. It is observed that both the peak frequencies shift toward the high frequency side with increase in temperature. At higher temperatures only a single peak has been

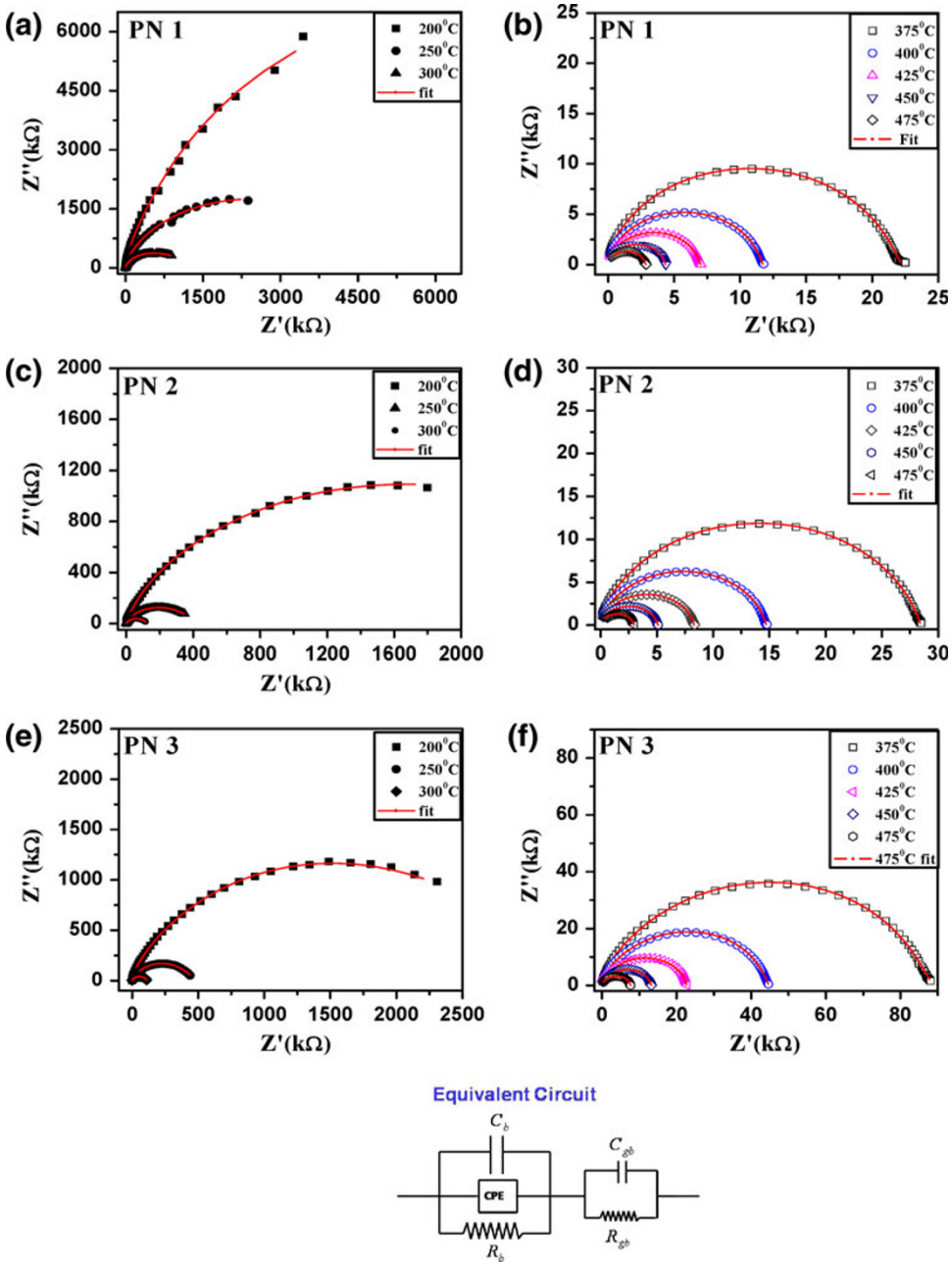

Fig. 6 Complex impedance plot (*symbol*), fitted data (*solid line*), and equivalent circuit of $(1 - x)$ $PbZr_{0.53}Ti_{0.47}O_3$–x $Ni_{0.65}Zn_{0.35}Fe_2O_4$ at various temperatures for different value of x. **a**, **b** $x = 0.10$, **c**, **d** $x = 0.20$ and **e**, **f** $x = 0.30$

observed. These peaks indicate the transition from long-range- to short-range mobility with increase in frequency. At the low frequency (of the peak) the ions are capable of moving a long distance (i.e., performing successful hopping from one site to the neighboring site). But for the high frequency side of peak, the ions are spatially confined to their potential wells and can execute only localized motion within the well (Pradhan et al. 2009). The appearance of two peaks in M'' versus frequency plots again confirms the presence of both grain and grain boundary effect in the material. These capacitances of different contributor (grain and grain boundary) are comparable even with the large difference between two resistance contributions. So, two resolved peaks are observed in M'' versus frequency plots. All the peaks are well resolved. The peak indicates the conductivity relaxation in material.

Figure 9 shows the frequency dependence of electrical conductivity (σ_{ac}) of the composites at different temperatures. At low temperatures, the conductivity pattern exhibits both low and high frequency dispersion (not shown in the figure). With rise in temperature, low-frequency independent conductivity plateau has been observed, where as high frequency dispersion of conductivity feature is still retained. The ac conductivity behavior obeys the Jonscher's power law governed by the relation (Jonscher 1983): $\sigma(\omega) = \sigma_{dc} + A\omega^n$ $(0 < n < 1)$, where σ_{dc} is the frequency-independent

Table 2 Comparison of temperature dependence of electrical parameters obtained from the fitting using the equivalent circuit model to the measured data at different temperatures (R_b (Ω), C_b (F), R_{gb} (Ω) and C_{gb} (F)) of $(1-x)$ $PbZr_{0.53}Ti_{0.47}O_3$–x $Ni_{0.65}Zn_{0.35}Fe_2O_4$ composites

Temperature→		400 °C	425 °C	450 °C	475 °C
Composition↓					
$x = 0.10$	R_b	11,240	6,625	4,014	1,343
PN 1	C_b	2.194×10^{-10}	2.353×10^{-10}	2.325×10^{-10}	2.848×10^{-10}
	R_{gb}	512.8	416	372.4	1,547
	C_{gb}	1.13×10^{-9}	9.824×10^{-10}	8.148×10^{-10}	3.924×10^{-10}
$x = 0.20$	R_b	14,040	7,835	2,800	1,687
PN 2	C_b	1.463×10^{-10}	1.572×10^{-10}	1.768×10^{-10}	1.884×10^{-10}
	R_{gb}	683.8	481.7	2,312	1,320
	C_{gb}	8.103×10^{-10}	7.487×10^{-10}	5.407×10^{-10}	5.215×10^{-10}
$x = 0.30$	R_b	18,340	21,650	12,390	3,424
PN 3	C_b	1.328×10^{-10}	9.27×10^{-10}	1.046×10^{-10}	1.491×10^{-10}
	R_{gb}	26,550	1,066	776.7	4,278
	C_{gb}	3.407×10^{-10}	5.241×10^{-10}	5.011×10^{-10}	3.479×10^{-10}

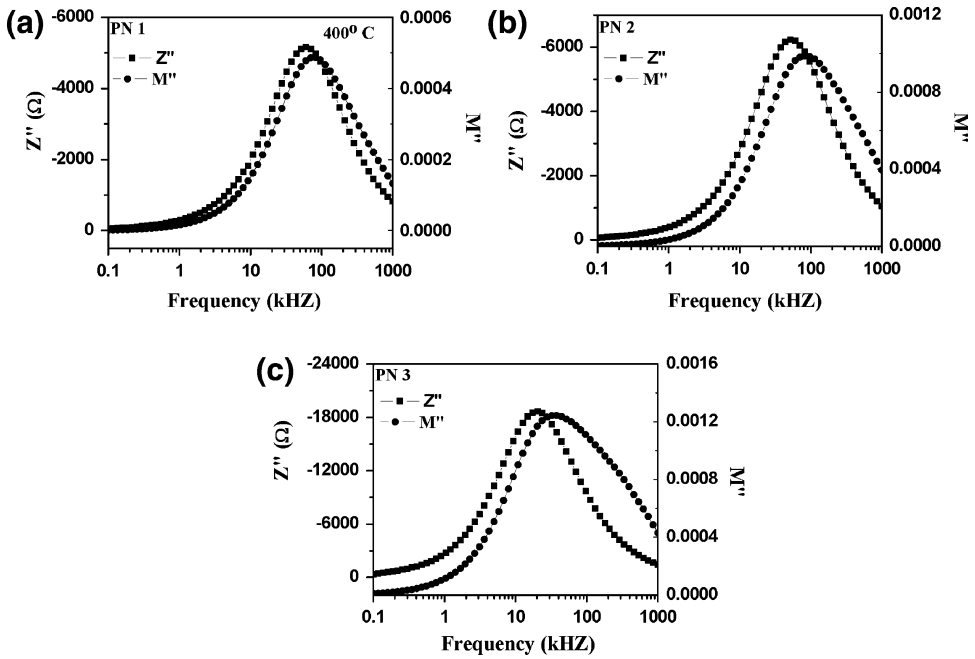

Fig. 7 Variation in Z'' and M'' with frequency at a particular temperature of $(1-x)$ $PbZr_{0.53}Ti_{0.47}O_3$–x $Ni_{0.65}Zn_{0.35}Fe_2O_4$ composites for different value of $x =$ **a** 0.10, **b** 0.20 and **c** 0.30

conductivity, A is the temperature-dependent pre-factor and n is the frequency exponent. In the figures, the symbols represent the experimental data and the solid line represents the fitted data employing Jonscher's power law. There is a close agreement between the experimental and fitted data. At higher temperatures, the high frequency dispersion corresponds to the ac conductivity and the low frequency plateau corresponds to the dc conductivity of the material. The frequency at which the change in the slope takes place is known as "hopping frequency (ω_p)". The hopping frequency is found to shift toward the higher temperature on increasing the temperature.

For conclusive evidence of the presence of spontaneous polarization, we have performed polarization versus electric field $||P$–$E|$ measurements, which exhibit a clear FE hysteresis for all the three samples, PN 1, PN 2, PN 3. Figure 10a, b and c clearly shows the ferroelectric hysteresis loops of the composites at room temperature confirming the ferroelectric properties of these composites. For $x = 0.1$ composite (PN 1), we have obtained reasonably high value of remanent polarization of $P_r = 0.18$ μC/cm^2 and coercive field $E_c = 11.7$ kV/cm. For PN 2 and PN 3 samples those values are 0.16 and 0.06 μC/cm^2 and 7.3 and 4.9 kV/cm, respectively. The remanent polarization and coercive field decrease with increase in NZFO content in the PZT matrix.

To understand the magnetic nature of $x = 0.1$, 0.2 and 0.3, composites showing magnetization as a function of

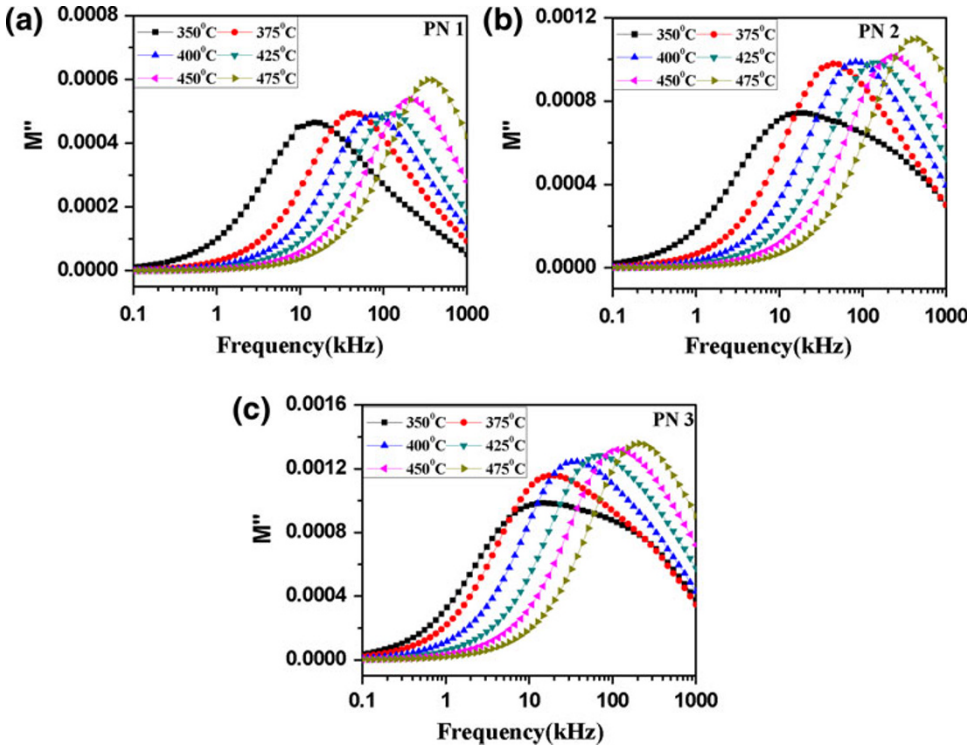

Fig. 8 Variation of imaginary part of complex modulus (M'') with frequency at various temperatures of $(1 - x)$ $PbZr_{0.53}Ti_{0.47}O_3$–x $Ni_{0.65}Zn_{0.35}Fe_2O_4$ composites for different value of x. **a** $x = 0.10$, **b** 0.20 and **c** 0.30

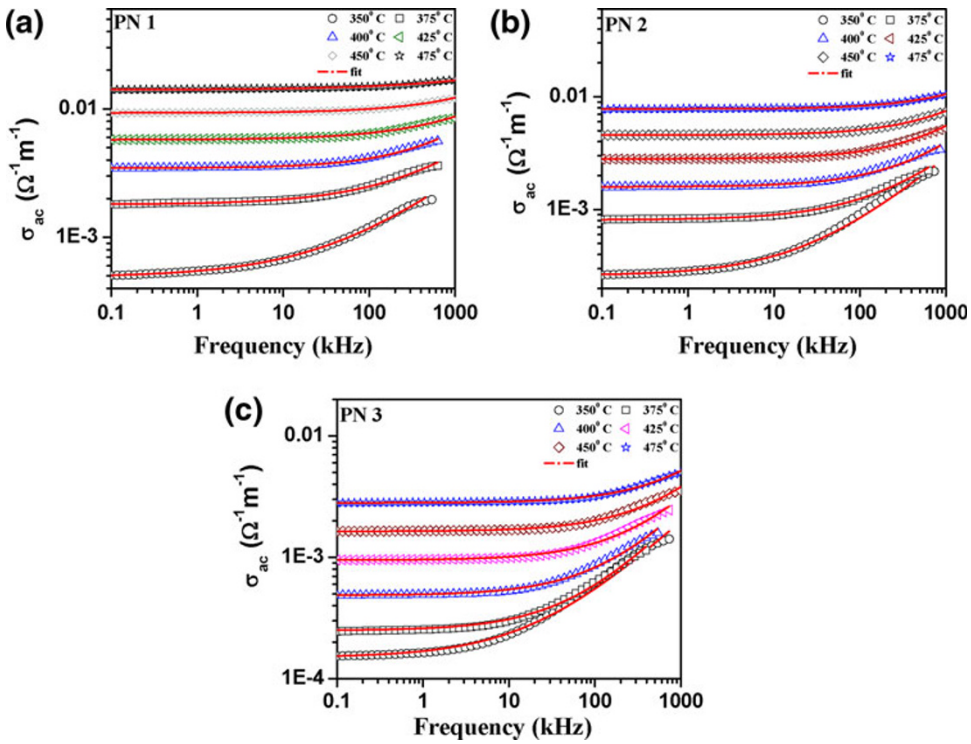

Fig. 9 Variation of ac conductivity (σ_{ac}) with frequency (*symbol*), fitted data (*solid line*) at different temperatures of $(1 - x)$ $PbZr_{0.53}Ti_{0.47}O_3$–x $Ni_{0.65}Zn_{0.35}Fe_2O_4$ composites for three different values of x. **a** $x = 0.10$, **b** 0.20 and **c** 0.30

magnetic field (hysteresis loops) at three different temperatures have been measured as shown in Fig. 11. The evaluated values of coercivity and remanent magnetization for these composites PN (1–3) at different temperatures (80–280 K) are summarized in Table 3. All the magnetization hysteresis loops (Fig. 11) are having a non-saturating nature as the applied maximum field is not very high. However, the M–H behavior of the composites undoubtedly indicates the presence of expected ferrimagnetism in the composite (due to the presence of NZFO with

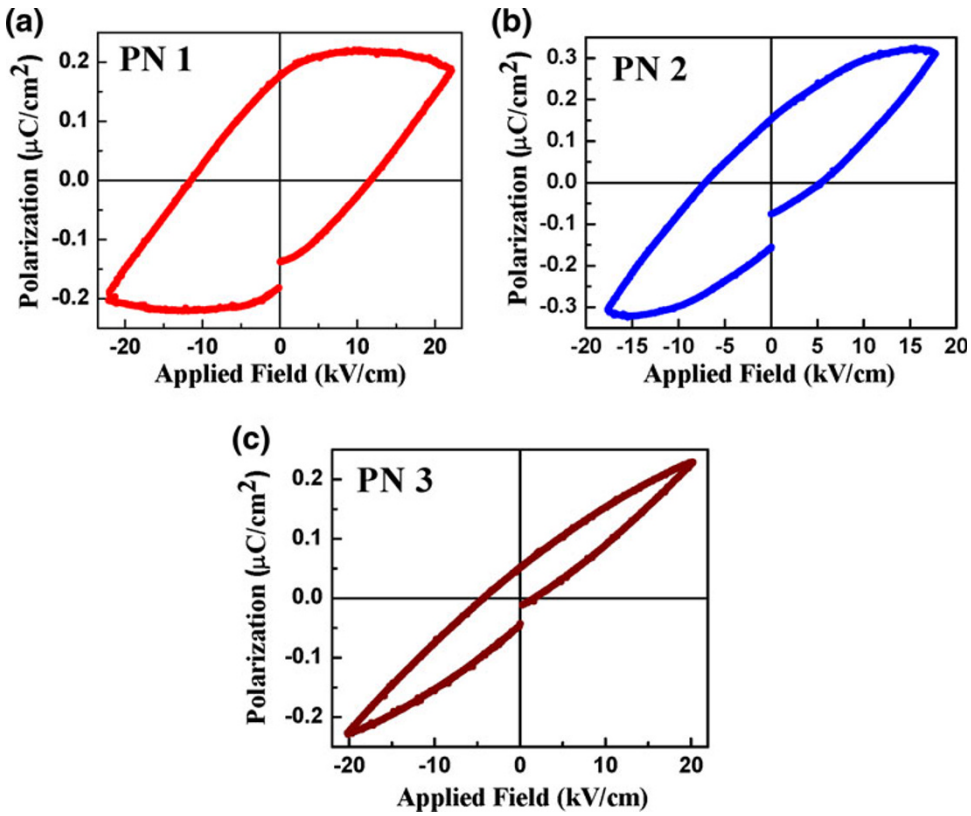

Fig. 10 *P–E* hysteresis loops of $(1 - x)$ $PbZr_{0.53}Ti_{0.47}O_3$–x $Ni_{0.65}Zn_{0.35}Fe_2O_4$ composites for three different values of x. **a** $x = 0.10$, **b** 0.20 and **c** 0.30 at room temperature showing ferroelectric behavior of the composites

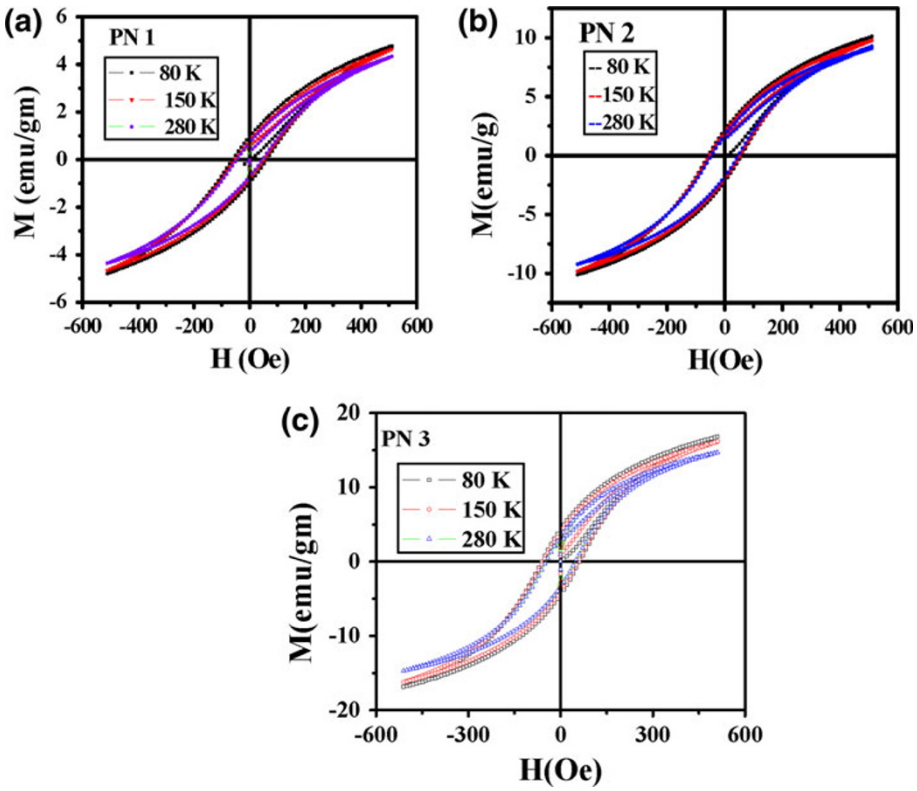

Fig. 11 *M–H* hysteresis loops of $(1 - x)$ $PbZr_{0.53}Ti_{0.47}O_3$–x $Ni_{0.65}Zn_{0.35}Fe_2O_4$ composites for x. **a** $x = 0.10$, **b** 0.20 and **c** 0.30 at different temperatures showing ferromagnetic nature of the composites

different percentages) showing an appreciable coercivity (~67.5 Oe at 80 K) and remanent magnetization (4.27 emu/g at 80 K). From Table 3, it is clear that as the concentration of NZFO is increased the H_c and M_r also increase. The H_c and M_r slightly decrease with the increase in temperature. For a pure nano-particle system of NZFO a

Table 3 Coercivity (H_c) and remanent magnetization (M_r) of $(1 - x)$ $PbZr_{0.53}Ti_{0.47}O_3$–x $Ni_{0.65}Zn_{0.35}Fe_2O_4$ (PN 1, PN 2 and PN 3) composites at different temperatures

Samples	80 K		150 K		280 K	
	H_c (Oe)	M_r (emu/gm)	H_c (Oe)	M_r (emu/gm)	H_c (Oe)	M_r (emu/gm)
PN 1	58.01	1.0	52.17	0.83	49.12	0.81
PN 2	60.11	2.26	55.04	1.97	50.11	1.73
PN 3	67.57	4.72	59.70	4.24	51.51	3.51

similar small value of coercivity employing similar preparation technique, has already been reported (Rao 2007; Khomchenko et al. 2008). So we conclude that in the composites (with the present phase proportion) the coercivity of NZFO has not changed considerably. We also predict that in our sample the magnetic interaction between the NZFO grains is weak as the NZFO grains are supposed to be surrounded by PZT having a high percentage of this material (PZT) in the composite. This effectively increases the distance between the magnetic grains (NZFO) and thereby reduces the interaction strength.

Conclusions

A different kind of good quality of PZT–NZFO multiferroic composites was synthesized using powder-in-sol precursor hybrid processing route. Detailed analysis of X-ray diffraction data revealed the presence of both PZT and NZFO immiscible phases (binary phase) in the PZT–NZFO composites. SEM micrographs show the non-uniform distribution of micron-sized NZFO particles in PZT matrix. Dielectric constant (ε_r) as a function of temperature reveals the paraelectric–FE transition temperature at $\sim$408 °C having maximum value of ε_r at the peak [$\varepsilon_r^{max} = 1{,}200$] with another low temperature anomaly at $\sim$297 °C, very close to the magnetic Curie temperature of the NZFO ferrite ($T_c = 300$ °C) for the $x = 0.1$ FE–FM composite. This new low temperature anomaly in dielectric measurement of this ferroelectric composite is confirmed to be very close to its magnetic transition (Curie) temperature, which strongly suggests reasonably high magnetoelectric coupling in these PZT/NZFO composites. Complex impedance spectroscopy analysis showed the contribution of both grain and grain boundary effects on the electrical properties of these composites. Frequency dependent of ac conductivity curves obey Jonscher's power law features very well. At higher temperatures, a low-frequency independent plateau is observed, whereas in the higher frequency region dispersion of conductivity is still retained. The crossover from the frequency-independent region to the frequency-dependent regions shows the onset of the conductivity relaxation, indicating the transition from long-range hopping to the short-range ionic motion. Polarization (P) versus electric field (E) studies at 300 K give conclusive evidence of the presence of spontaneous polarization in all the three composites ($x = 0.1$, 0.2 and 0.3). However, area of P–E loop, coercive field (E_c) and remanent polarization (P_r) are found to decrease noticeably with the increase of the NZFO content (x) in these composites.

From the temperature-dependent magnetization hysteresis (M–H) loop studies of the PZT/NZFO composite, it confirms excellent non-saturating ferrimagnetic behavior with increase in both coercive field (H_c) and remanent magnetization (M_r) when the NZFO content in the composite is increased. H_c and M_r slightly decrease with the increase in temperature. We have optimized the weight percent of ferrimagnetic NZFO ferrite and ferroelectric PZT in the composite to attain sustained simultaneous FM and FE properties. Our study showed that a different kind multiferroics with composite character obtained by artificial combination of different materials can attain excellent ferroelectric and magnetic (ferrimagnetic) properties which the individual components by themselves cannot attain. Further study can be initiated to investigate magnetoelectric coupling directly in these multiferroic composites.

Acknowledgments The authors would like to acknowledge gratefully the financial support of Department Science and Technology (DST), New Delhi, India, through Project No. IR/S2/PU-04/2006.

References

Catlan G, Scott JF (2009) Physics and applications of bismuth ferrite. Adv Mater 21:2463

Chen W, Wang ZH, Ke C, Zhu W, Tan OK (2009) Preparation and characterization of $Pb(Zr_{0.53}Ti_{0.47})O_3/CoFe_2O_4$ composite thick films by hybrid sol–gel processing. Mater Sci Eng B 162:47

Chen W, Shannigrahi S, Chen XF, Wang ZH, Zhu W, Tan OK (2010a) Multiferroic behavior and magnetoelectric effect in $CoFe_2O_4/Pb(Zr_{0.53}Ti_{0.47})O_3$ thick films. Solid State Commun 150:271

Chen W, Zhu W, Ke C, Yang Z, Wang L, Chen XF, Tan OK (2010b) Impedance spectroscopy and conductivity mechanism of $CoFe_2O_4$–$Pb(Zr_{0.53}Ti_{0.47})O_3$ composite thick films. J Alloy Compd 508:141

Choudhary RNP, Pradhan DK, Tirado CM, Bonilla GE, Katiyar RS (2006) Relaxor characteristics of $Pb(Fe_{2/3}W_{1/3})O_3$–$BiFeO_3$ solid solution prepared by mechanosynthesis route. J Appl Phys 100: 084105

Chougule SS, Patil DR, Chougule BK (2008) Electrical conduction and magnetoelectric effect in ferroelectric rich $(x)Ni_{0.9}Zn_{0.1}Fe_2O_4 + (1 - x)$PZT ME composites. J Alloy Compd 452: 205–209

Eerenstein W, Mathur ND, Scott JF (2006) Multiferroic and magnetoelectric materials. Nature 442:759

Fawzi AS, Sheikh AD, Mathe VL (2010) Multiferroic properties of Ni ferrite–PLZT composite. Physica B 405:340

Harnagea C, Mitoseriu L, Buscaglia V, Pallecchi I, Nanni P (2007) Magnetic and ferroelectric domain structures in $BaTiO_3$–$(Ni_{0.5}Zn_{0.5})Fe_2O_4$ multiferroic ceramics. J Eur Ceram Soc 27:3947

Jonscher AK (1983) Dielectric relaxation in solids. Chelsea Dielectric Press, London

Kao KC (1992) Dielectric phenomena in solids, Marcel Dekker, New York, pp 41–69

Khomchenko VA, Kiselev DA, Vieira JM, Jian L, Kholkin AL, Lopes AML, Pogorelov YG, Araujo JP, Maglione M (2008) Effect of diamagnetic Ca, Sr, Pb, and Ba substitution on the crystal structure and multiferroic properties of the $BiFeO_3$ perovskite. J Appl Phys 103:024105

Lanfredi S, Carvalho JF, Hernandes AC (2000) Electric and dielectric properties of $Bi_{12}TiO_{20}$ single crystals. J Appl Phys 88:283

Lee YH, Wu JM, Lai CH (2006) Influence of La doping in multiferroic properties of $BiFeO_3$ thin films. Appl Phys Lett 88:042903

Liu M, Li X, Imrane H, Chen Y (2007) Synthesis of ordered arrays of multiferroic $NiFe_2O_4$-$Pb(Zr_{0.52}Ti_{0.48})O_3$ core-shell nanowires. Appl Phys Lett 90:152501

Ma YG, Cheng WN, Ning M, Ong CK (2007) Magnetoelectric effect in epitaxial $Pb(Zr_{0.52}Ti_{0.48})O_3/La_{0.7}Sr_{0.3}MnO_3$ composite thin film. Appl Phys Lett 90:152911

Macdonald JR (1984) Note on the parameterization of the constant-phase admittance element. Solid State Ionics 13:147

Macdonald JR (1987) Impedance spectroscopy, emphasizing solid materials and systems. Wiley, New York

Mangalaraja RU, Ananthakumar S, Manohar P, Gnanam FD (2002) Magnetic, electrical and dielectric behaviour of $Ni_{0.8}Zn_{0.2}Fe_2O_4$ prepared through flash combustion technique. J Magn Magn Mater 253:56

Martin LW, Crane SP, Chu YH, Holcomb MB, Gajek M, Huijben M, Yang CH, Balke N, Ramesh R (2008) Multiferroics and magnetoelectrics: thin films and nanostructures. J Phys Condens Matter 20:434220

Martínez R, Kumar A, Palai R, Katiyar RS, Scott JF (2010) Study of physical properties of integrated ferroelectric/ferromagnetic heterostructures. J Appl Phys 107:114107

Mathews S, Ramesh R, Venkatesan T, Benedetto J (1997) Ferroelectric field effect transistor based on epitaxial perovskite heterostructures. Science 276:238

Miao J, Cao L, Yuan J, Chen W, Yang H, Xu B, Qiu X, Zhao B (2005) Microstructure dependence of the electrical properties of $(Ba,Sr)TiO_3$ thin film deposited on $(La,Sr)MnO_3$ conductive layer. J Cryst Growth 276:498

Ortega N, Kumar A, Bhattacharya P, Majumder SB, Katiyar RS (2008) Impedance spectroscopy of multiferroic $PbZr_xTi_{1-x}O_3$/$CoFe_2O_4$ layered thin films. Phys Rev B 77:014111

Pradhan DK, Choudhary RNP, Rinaldi C, Katiyar RS (2009) Effect of Mn substitution on electrical and magnetic properties of $Bi_{0.9}La_{0.1}FeO_3$. J Appl Phys 106:024102

Prellier W, Singh MP, Murugavel P (2005) The single-phase multiferroic oxides: from bulk to thin film. J Phys Condens Matter 17:R803

Ramesh R, Spaldin NA (2007) Multiferroics: progress and prospects in thin films. Nat Mater 6:21

Rao P, Rao GSN, Mahesh Kumar A, Rao KH, Murthy YLN, Hong SN, Kim C-O, Kim CG (2007) Soft chemical synthesis and characterization of $Ni_{0.65}Zn_{0.35}Fe_2O_4$ nanoparticles. J Appl Phys 101:123902

Ryu S, Park JH, Jang HM (2007) Magnetoelectric coupling of [00l]-oriented $Pb(Zr_{0.4}Ti_{0.6})O_3$–$Ni_{0.8}Zn_{0.2}Fe_2O_4$ multilayered thin films. Appl Phys Lett 91:142910

Singh MP, Prellier W, Mechin L, Raveau B (2006) Effect of ferroelectric layers on the magnetocapacitance properties of superlattices-based oxide multiferroics. Appl Phys Lett 88:012903

Spaldin NA, Fiebig M (2005) The renaissance of magnetoelectric multiferroics. Science 309:391

Uchino K (2000) Ferroelectric devices. Marcel Dekker, New York, pp 221–240

Vaz CAF, Segal Y, Hoffman J, Grober RD, Walker FJ, Ahn CH (2010) Temperature dependence of the magnetoelectric effect in $Pb(Zr_{0.2}Ti_{0.8})O_3/La_{0.8}Sr_{0.2}MnO_3$ multiferroic heterostructures. Appl Phys Lett 97:042506

West AR, Sinclair DC, Hirose N (1997) Characterization of electrical materials, especially ferroelectrics, by impedance spectroscopy. J Electroceramics 1:65–71

Wu Y, Wan J, Huang C, Weng Y, Zhao S, Liu J, Wang G (2008) Strong magnetoelectric coupling in multiferroic $BiFeO_3$–$Pb(Zr_{0.52}Ti_{0.48})O_3$ composite films derived from electrophoretic deposition. Appl Phys Lett 93:192915

Yan L, Wang Z, Xing Z, Li J, Viehlan D (2010) Magnetoelectric and multiferroic properties of variously oriented epitaxial $BiFeO_3$–$CoFe_2O_4$ nanostructured thin films. J Appl Phys 107:064106

Zhang H, Or SW, Chan HLW (2008) Multiferroic properties of $Ni_{0.5}Zn_{0.5}Fe_2O_4$–$Pb(Zr_{0.53}Ti_{0.47})O_3$ ceramic Composites. J Appl Phys 104:104109

Zhang H, Or SW, Chan HLW (2009) Fine-grained multiferroic $BaTiO_3/(Ni_{0.5}Zn_{0.5})Fe_2O_4$ composite ceramics synthesized by novel powder-in-sol precursor hybrid processing route. Mater Res Bull 44:1339

Zheng H, Wang J, Lofland SE, Ma Z, Mohaddes-Ardabili L, Zhao T, Salamanca-Riba L, Shinde SR, Ogale SB, Bai F, Viehland D, Jia Y, Schlom DG, Wuttig M, Roytburd A, Ramesh R (2004) Multiferroic $BaTiO_3$-$CoFe_2O_4$ nanostructures. Science 303:661